DOI: 10.1002/chem.200601704

Formation of the Active Species of Cytochrome P450 by Using Iodosylbenzene: A Case for Spin-Selective Reactivity

Kyung-Bin Cho,[a] Yohann Moreau,[a] Devesh Kumar,[a, b] Dan A. Rock,[c, d] Jeffrey P. Jones,*[c] and Sason Shaik*[a]

Abstract: The generation of the active species for the enzyme cytochrome P450 by using the highly versatile oxygen surrogate iodosylbenzene (PhIO) often produces different results compared with the native route, in which the active species is generated through O_2 uptake and reduction by NADPH. One of these differences that is addressed here is the deuterium kinetic isotope effect (KIE) jump observed during N-dealkylation of *N*,*N*-dimethylaniline (DMA) by P450, when the reaction conditions change from the native to the PhIO route. The paper presents a theoretical analysis targeted to elucidate the mechanism of the reaction of PhIO with heme, to form the high-valent iron–oxo species Compound I (Cpd I), and define the origins of the KIE jump in the reaction of Cpd I with DMA. It is concluded that the likely origin of the KIE jump is the spin-selective chemistry of the enzyme cytochrome P450 under different preparation procedures. In the native route, the reaction proceeds via the doublet spin state of Cpd I and leads to a low KIE value. PhIO, however, diverts the reaction to the quartet spin state of Cpd I, which leads to the observed high KIE values. The KIE jump is reproduced here experimentally for the dealkylation of *N*,*N*-dimethyl-4-(methylthio)aniline, by using intramolecular KIE measurements that avoid kinetic complexities. The effect of PhIO is compared with *N*,*N*-dimethylaniline-*N*-oxide (DMAO), which acts both as the oxygen donor and the substrate and leads to the same KIE values as the native route.

Keywords: cytochromes · density functional calculations · heme proteins · kinetic isotope effects · spin selectivity

Introduction

The cytochrome P450 family of enzymes is well known for mediating oxygenation reactions on a plethora of diverse chemical structures.[1–5] Targeting a range of substrates, the enzyme utilizes a heme group for its catalysis, normally with consumption of O_2 and reducing equivalents supplied ultimately from NADPH (hereafter, the "native route"). Central to this reaction is an oxidizing species that is subject to many ongoing studies today.[3–5] In the late 1970s, it was shown that this oxidizing species, or at least one that functions like it, could be generated by oxygen atoms derived from $NaIO_4$ and $NaClO_2$ that serve as "oxygen surrogates" in the absence of O_2 and NADPH.[6–8] Subsequently, Lichtenberger et al.[9] reported on iodosylbenzene (PhIO)-supported liver microsomal O-dealkylation of 7-ethoxycoumarin without NADPH or O_2. Around the same time, Gustafsson and Bergman[10] showed that PhIO is an efficient oxygen donor that supports hydroxylation of fatty acids. PhIO was thus found to be a very efficient oxygen donor for the reaction, and the formation of the oxidizing species. Due to the nature of the oxygen donors, it could be assumed that

[a] Dr. K.-B. Cho, Dr. Y. Moreau, Dr. D. Kumar, Prof. S. Shaik
Department of Organic Chemistry and
The Lise Meitner-Minerva Center for Computational Quantum Chemistry
Hebrew University, 91904 Jerusalem (Israel)
Fax: (+972) 2-6584680
E-mail: sason@yfaat.ch.huji.ac.il

[b] Dr. D. Kumar
Current address:
Max-Planck-Institut für Kohlenforschung
Kaiser-Wilhelm-Platz 1, 45470 Mülheim an der Ruhr (Germany)

[c] Dr. D. A. Rock, Prof. J. P. Jones
Department of Chemistry, Washington State University
PO BOX 644630, Pullman, WA 99164-4630 (USA)
Fax: (+1) 509-335-8867
E-mail: jpj@wsu.edu

[d] Dr. D. A. Rock
Current address:
Amgen, Pharmacokinetics & Drug Metabolism
1201 Amgen Court West, Seattle, WA 98119 (USA)

Supporting information for this article is available on the WWW under http://www.chemeurj.org/ or from the author.

the P450 oxidizing species contained only one oxygen atom, thereby strengthening the conjecture that this species was related to Compound I (Cpd I) found in horseradish peroxidase (HRP).[6,7] Recently, Dowers et al.[11] have shown that the single oxygen atom donated from *N*-oxide of three different substituted *N*,*N*-dimethylanilines (DMAs) gives identical isotope effects for N-dealkylation as the enzyme system supported by NADPH and O_2, supporting the idea that a single oxygen atom is the oxidizing species for this reaction. Thus, there is a general consensus today that the active species is indeed the high-valent iron–oxo species Cpd I, which is directly responsible for the oxygenation of substrates in P450 oxidations. Indeed, while the active-oxygen species has evaded experimental detection, since the rate-limiting step precedes its formation leading to low steady-state levels of Cpd I under the native conditions, its involvement in the reaction has been strongly inferred.[4,11] The similarity between the oxidizing species generated with PhIO and the NADPH/O_2-generated Cpd I has been documented,[12,13] and Cpd I is now presumed to be formed with PhIO as well. Moreover, given that the rate-limiting step in the generation of Cpd I by NADPH and O_2 is the second electron transfer from P450 reductase, the iodosylbenzene procedure bypasses this step and is thus better suited for studies of the reaction of Cpd I with substrates. As such, PhIO has become an important mechanistic tool in the study of heme enzymes in both substrate oxidation and inhibition mechanisms.[14,15]

For instance, given the ability of PhIO to circumvent any dioxygen species in the catalytic cycle of P450, the reagent has been used to distinguish between oxidations by Cpd 0 (an iron–peroxy species) and Cpd I.[16–18] Since Cpd 0 has been suggested as an additional P450 oxidant,[19] the detection of differences between surrogate single oxygen donors and the native route have often been taken as evidence for the functioning of Cpd 0 (or a similar species) alongside Cpd I. As such, PhIO has also been used to circumvent the rate-limiting second electron reduction, and by difference with the native route, served to pin down the effects of steps prior to oxidation, and their contribution to the preexponential factor.[20] Furthermore, since PhIO eliminates the need for P450 reductase, its utilization provided an assessment of the role of protein–protein interactions in altering reaction regioselectivity through conformational changes in the P450 enzyme.[21] Finally, its utility is wide-ranging and stretches beyond the heme system to nonheme mimetic systems in bioinorganic chemistry, in which it can be utilized to synthesize novel high-valent metal–oxo reagents.[22] PhIO is often used to generate Cpd I in model systems that are compared with the P450 enzyme native route. All of these applications depend on the Cpd I species that is generated by the native route and by PhIO being identical.

In light of this widespread use, it has become important to understand the differences in Cpd I species generated by PhIO and other oxygen donors with respect to the NADPH/O_2-generated Cpd I. Minor differences were noted early on,[13,23] but more recently, evidence has been accumulating that the oxidant generated by the reaction of PhIO with P450 behaves differently compared with the Cpd I generated by the native route. Guengerich et al.[24] showed that the application of PhIO generated an oxidizing species that leads to considerably higher kinetic isotope effect (KIE) compared with the natively generated Cpd I, and much more like the KIE observed from the reaction with HRP. This was attributed to a possible formation of a PhI-O-Fe complex[25] that generated a protonated Cpd I less capable of abstracting the proton from the substrate. The notion of a PhI-O-Fe oxidizing complex was supported by Collman et al.,[26,27] who used different iodosylarenes as oxygen donors, and showed that these reagents gave different product ratios for epoxidation of substrates. This was inconsistent with the view that beyond the formation of Cpd I, the initial source of oxygen did not matter for the reactions. A PhI-O-Fe complex was indeed found by Nam et al.[28,29] to be in equilibrium with Cpd I, but whether or not this complex was an oxidizing species could not be ascertained by the experimental data. Recently, Bhakta et al.[18] have shown that the PhIO-generated oxidant differs from the normal Cpd I in dealkylating *N*-cyclopropyl-*N*-alkyl-*p*-chloroaniline derivatives, yielding different products. In fact, the PhIO-generated Cpd I produced the same products as HRP.

Taken together, there is enough evidence to conclude that the Cpd I formation from oxygen donors such as PhIO is not well understood, and experiments may have been conducted for some time under the potentially inaccurate assumption that PhIO-generated Cpd I would behave the same way as the native Cpd I. Along with the fleeting existence of Cpd I, this situation creates an ideal situation for computational research directed at understanding the mechanism of formation of Cpd I from oxygen donors or surrogates. We have therefore conducted a theoretical investigation of the reactions of the two oxygen surrogates, outlined in Scheme 1, in

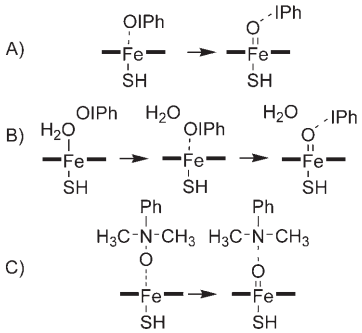

Scheme 1. The three reactions investigated in this study.

an attempt to understand the reason why the use of PhIO (reactions A and B) leads to a KIE jump,[24] while the use of *N*,*N*-dimethylaniline-*N*-oxide (DMAO), in reaction C, leads to low KIE values, identical to those obtained from the native route of the enzyme, for a few different P450 isoforms.[11] To rule out that the KIE jumps originated in "kinetic complexity", we also carried out experiments with PhIO to ascertain the KIE jump by determining intramolec-

ular KIE values for N-dealkylation of *N*,*N*-dimethyl-4-(methylthio)aniline. Since we have shown in the past that *N*-methyl-*N*-(trideuteromethyl)anilines exhibit kinetic complexity ("masking") and do not provide a good estimate of the intrinsic isotope effect for some P450 enzymes,[30] we adapted here a special experimental design. The deutrium content of the formaldehyde produced from *N*,*N*-bis(dideuteromethyl-^{13}C)-4-(methylthio)aniline is used to determine the intramolecular isotope effect; thereby evading the masking issue (see more later).

Results

Three model reactions were investigated in this study. In all of the models, the heme is represented by an iron–porphine ring, and an SH group replaces the axial cysteine ligand which is present in P450. In the first reaction (reaction A, Scheme 1), we studied the simple process in which PhIO binds to pentacoordinate heme and Cpd I is formed through oxygen transfer. In the second reaction (reaction B, Scheme 1), this system was extended to include a water ligand to represent the aqua–ferric resting state of the P450 enzyme (note that in the enzyme there is a spin equilibrium between low- and high-spin species; the latter is pentacoordinated). Thus in the second case the reaction involves the displacement of the water ligand from the heme before the binding of PhIO. In the third reaction (reaction C, Scheme 1), DMAO has been used as the oxygen donor in order to further confirm and correlate the conclusions obtained from reactions A and B to experimental results. The energy values mentioned throughout this study include big basis set, solvent, and zero-point vibration energy (Z_0) corrections unless explicitly otherwise stated. Thermal effects, that is, entropy and enthalpy corrections, are only included where specifically mentioned.

Reaction A: The ground state of the pentacoordinate heme was found to be the sextet spin state, with the valence-electron orbital configuration of $(\delta)^1(\pi^*_{yz})^1(\pi^*_{xz})^1(\sigma^*_{z^2})^1(\sigma^*_{xy})^1$, all electrons having a spin-up configuration. These results have previously been obtained for the pentacoordinated heme models tested before.[31–33] The energy difference to the quartet state, with the configuration $(\pi^*_{xz})^1(\pi^*_{yz})^1(\sigma^*_{z^2})^1$ is 3.1 kcal mol^{-1} higher. The doublet state $(\pi^*_{yz})^1$, in contrast, lies considerably higher in energy at 7.3 kcal mol^{-1} over the sextet. The energies for reaction A are collected in Table 1.

Table 1. Relative energies[a] for the different structures in reaction A [data in kcal mol^{-1}].

	Heme +OIPh	**1**	**TS1**	**2**	Cpd I +IPh
doublet	7.15	0.00	5.06	−5.44	−3.98
quartet	2.95	2.11	7.72	−5.75	−3.75
sextet	−0.18	2.10	7.91	3.39	5.74

[a] These energies are obtained at B3LYP/LACV3P*$^+$(ERMLER2*$^+$ on I)//LACVP level, including Z_0 and solvent effects (see Computational methods).

However, upon PhIO binding to the heme (structure **1** in Figure 1a), all three states are now close to each other, within 2.1 kcal mol^{-1}, with the doublet state (^{2}**1**) being lowest. The various spin-states have the same orbital electronic configurations as in the pentacoordinate heme complex. Figure 1a shows the geometrical parameters for **1**. Consistent with the small binding energy, the O–Fe distance ranges from 1.9 to 2.2 Å. The I–O distance barely changes compared to the free PhIO (Table S17 in the Supporting Information), confirming the view that this species is more correctly described as a weak PhIO···heme complex and is not a PhI–Cpd I complex (i.e., PhI···O=FePor).

The transfer of the oxygen from PhIO to the heme and formation of Cpd I is found to occur through a transition

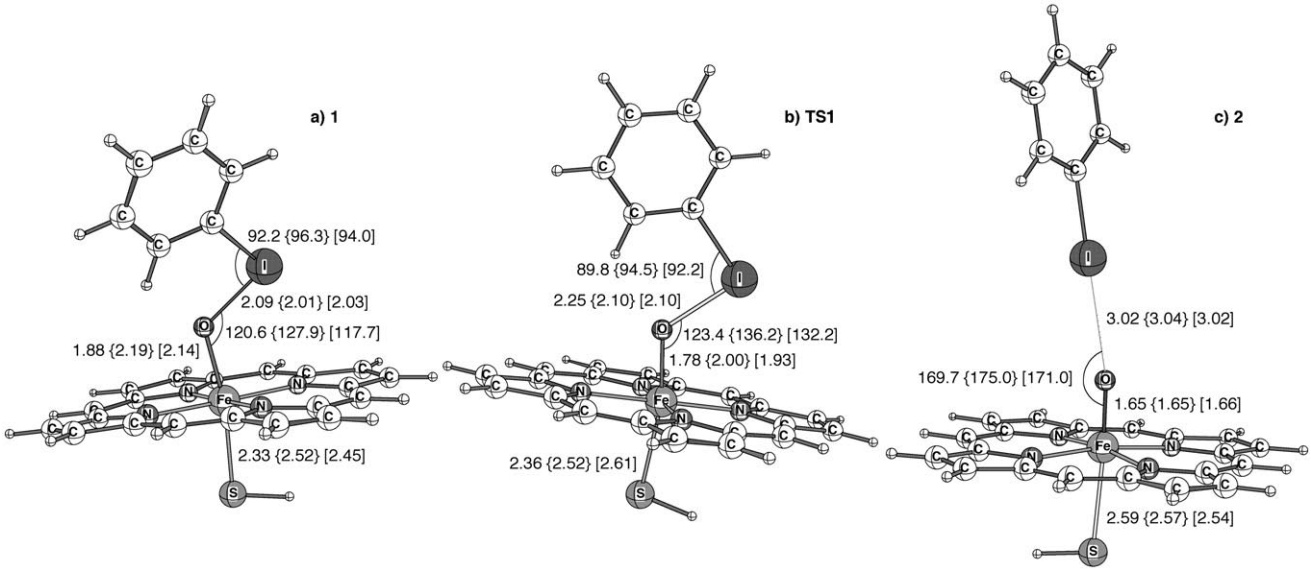

Figure 1. Optimized structure a) **1**, b) **TS1**, and c) **2** for reaction A. Values with two decimals are distances in Å. Values with one decimal are angles in degrees. The values for each species are in order doublet, {quartet}, and [sextet].

state (**TS1**, Figure 1b) with a moderate energy barrier ranging from 5.1 to 7.9 kcal mol^{-1}. This confirms that this reaction is faster than the normal generation of Cpd I, in which the O_2 bond breaking in general has a barrier in the range of 10–15 kcal mol^{-1}, and the rate-limiting electron-transfer step from the P450 reductase should correspond to an even higher barrier. The spin and charge distributions for this transition-state structure resemble more the corresponding features in **1** rather than **2** (compare Tables S5, S8, and S11), but the critical O–Fe distance half way between these two structures and the imaginary frequencies of 103.4*i*, 223.8*i*, and 184.6*i* cm^{-1}, in respective spin states, confirm that this is indeed a transition-state structure.

The product of this reaction (**2**) is shown in Figure 1c. The oxygen has now undergone bonding to the heme, forming Cpd I. The Cpd I state with Fe^{V} oxidation number on iron was not produced by the process, in accord with previous calculations showing this species to lie about 20 kcal mol^{-1} above the Por(+•)$Fe^{IV}O$ states.[34] As may be seen by inspection of structure **2**, the PhI moiety is bound very weakly to the oxygen with the I–O distance at around 3 Å. The PhI–Cpd I complexation energies are in the range 1.5–2.4 kcal mol^{-1} within respective multiplicities. Structures ^{2}**2** and ^{4}**2** are virtually degenerate and ^{6}**2** is 9.1 kcal mol^{-1} higher in energy than ^{4}**2**. These energy differences between the spin states of Cpd I are known from earlier calculations.[35–37]

A couple of interesting results relating to these calculations are worth mentioning. First, upon releasing **TS1** in the direction of the product **2**, the freed PhI would find a position alongside the porphine plane, where the protons of the porphine macrocycle can weakly hold it. In fact, the LACVP energies were virtually the same as **2**. Therefore, this distinction between **2** and the obtained complexed product was insignificant, other than to confirm that the I–O interaction at this stage is extremely weak, and that the surface may have multiple local minima. The weakness of the complexation interaction between PhI and Cpd I casts serious doubts on the suggestions that this is the root cause of the differences in the reactivity between the native route and the PhIO route.[24–27]

A second feature is that the sextet ^{6}**TS1** species found here in fact led to an iron–oxo product in which the sulfur ligand was detached from the iron atom. It should be noted, that this iron–sulfur bond disruption may or may not really happen in the real enzyme, for which the sextet state was found by QM/MM calculations to have a normal Fe–S bond.[35] In the current theoretical model, we assume that the detached sulfur returns to the axial ligand position. Indeed, by varying the Fe–S bond length, it is found that the Fe–S bond once again can form over a negligible barrier lying lower than ^{6}**TS1** (Figure S7 in the Supporting Information). Therefore, **TS1** is here presented as the transition state connecting **1** with **2**. Nevertheless, to be cautious we shall consider later also the putative consequences of this heme dissociation in the sextet state.

The main conclusions drawn from reaction A are that the energy barrier **TS1** is overall relatively low, and the differences are small between the different multiplicities at this point. Inclusion of thermal effects to the reaction reduces this gap even further (Table S28), and the higher multiplicities will even be lower in the presence of hydrogen bonds to sulfur (see below). The final energy graph of reaction A is shown in Figure 2.

Theoretical results on the effects of hydrogen bonds on sulfur: To investigate the effect of hydrogen bonds to the sulfur ligand on the overall energy, single-point calculations were carried out on **1**, **TS1**, and **2**, with two NH_3 molecules hydrogen bonded to the sulfur at a distance of 2.66 Å. No frequency calculations were done on these structures since they were not optimized; hence Z_0 is not included in any of the values quoted in this section, including those without the NH_3 molecules. The relative energy values are presented in Table 2.

The effect on the order of the different states was negligible for **2**, but it was more pronounced for **1** and **TS1**. Relative to ^{2}**1**, the relative energy of ^{4}**1** dropped from 3.3 to −2.2 kcal mol^{-1}, while ^{6}**1** went from 4.2 to 1.8 kcal mol^{-1}.

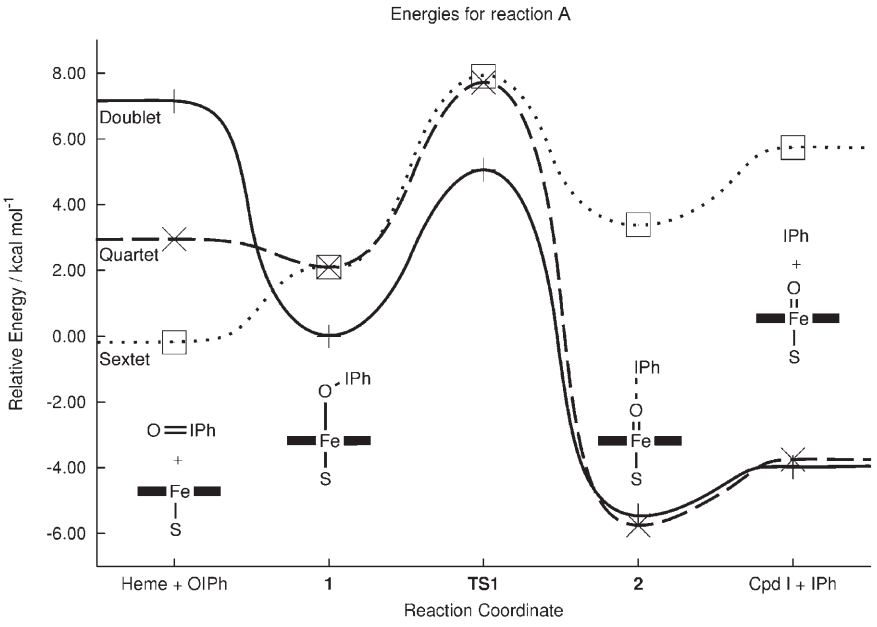

Figure 2. Energy changes of reaction A taken from Table 1. The values include single-point energies using the large basis set, solvation, and Z_0.

Table 2. Influence on the relative energies[a] by NH···S hydrogen bonding to SH ligand [data in kcal mol^{-1}].

	Without NH···S			With 2 NH···S		
	1	**TS1**	**2**	**1**	**TS1**	**2**
doublet	0.00	5.28	−5.35	0.00	3.73	−8.75
quartet	3.30	9.27	−5.58	−2.17	3.45	−8.50
sextet	4.22	10.54	5.01	1.77	4.97	1.62

[a] The relative energies correspond to B3LYP/LACV3P*$^{+}$ (ERMLER2*$^{+}$ on I)//LACVP and include solvent correction but not Z_0 correction.

This would reflect the hydrogen-bond effect on the populated $\sigma^*_{z^2}$ orbital for ^{4}**1** and ^{6}**1**,[33,37–39] which is not populated in the case of ^{2}**1** or **2**. This trend was continued in **TS1**. Specifically, it now predicts ^{4}**TS1** to be the lowest by 0.3 kcal mol^{-1} lower than ^{2}**TS1**. Comparing the relative energies of **1**, **TS1** , and **2** to each other, the extra hydrogen bonds increase the exothermicity for the doublet surface (from 5.4 to 8.8 kcal mol^{-1}), but this increase is largely compensated by the stabilization of ^{4}**1** and ^{6}**1** in the quartet and sextet surface. The barriers are also lowered by a small amount.

Based on these observations, it is clear that environmental factors play a role in this reaction. The important observation here is that hydrogen bonds to the thiolate ligand stabilize the higher multiplicities of **1** and **TS1** more than they stabilize the doublet state, as discussed later.

Reaction B: Adding a water molecule to the heme, the reaction starts with the resting state model of the enzyme with a water molecule ligated in the previously vacant axial position. Therefore, the reaction now includes a water dislocation step that occurs before the main reaction, the oxygen transfer to the iron, takes place. At the resting state, the heme–H_2O, all the spin states are energetically within 1.4 kcal mol^{-1} from each other. Upon complexation (structure **0**, Figure 3a) PhIO forms a hydrogen bond to the water. Energetically, ^{2}**0** is now lowest, but the states remain close to each other. The complexation energies are in the range 4.6–6.0 kcal mol^{-1} relative to ^{2}**0** (Table 3).

The dislocation of the water ligand occurs over a transition state **TS0** (Figure 3b). The water is now completely dissociated from the heme, and PhIO is about to bind to Fe. The region around this transition state is flat, with imaginary frequencies of 33.0*i*, 27.7*i*, and 25.9*i* cm^{-1} for the various spin states. The doublet state ^{2}**TS0** is now clearly the highest state at 9.2 kcal mol^{-1} (relative to ^{2}**1**), while ^{4}**TS0** is 3.3 kcal mol^{-1} (relative to ^{2}**0**). The sextet ^{6}**TS0** state on the other hand is associated with a very small barrier, only 0.6 kcal mol^{-1} above ^{2}**0**, which is also 0.6 kcal mol^{-1} lower than ^{6}**0**. Thus with such differences between the spin states, it can be concluded that the high energy ^{2}**TS0** acts as a "filter" that allows the reaction to go on in higher multiplicities in general, and hindering the reaction to occur at the doublet state in particular. The reason for the low energy of the sextet state at **TS0** and for the high energy of the doublet state is associated with the relative strength of Fe–OH_2 binding and is not particularly affected by PhIO, which is only loosely coordinated to the heme. Therefore, the energy profile for water dislocation is quite general, irrespective of the identity of the oxygen donor.

Table 3. Relative energies [in kcal mol^{-1}][a] for the different structures in reaction B.

	[H_2O–heme] +PhIO	**0**	**TS0**	**1**	**TS1**	**2**	[H_2O-CpdI] +PhI
doublet	6.90	0.85	9.18	0.00	6.25	−3.21	−3.09
quartet	6.37	2.32	4.17	1.84	8.29	−2.74	−3.88
sextet	5.48	2.04	1.42	1.75	8.68	4.87	4.70

[a] Energies obtained as in Table 1.

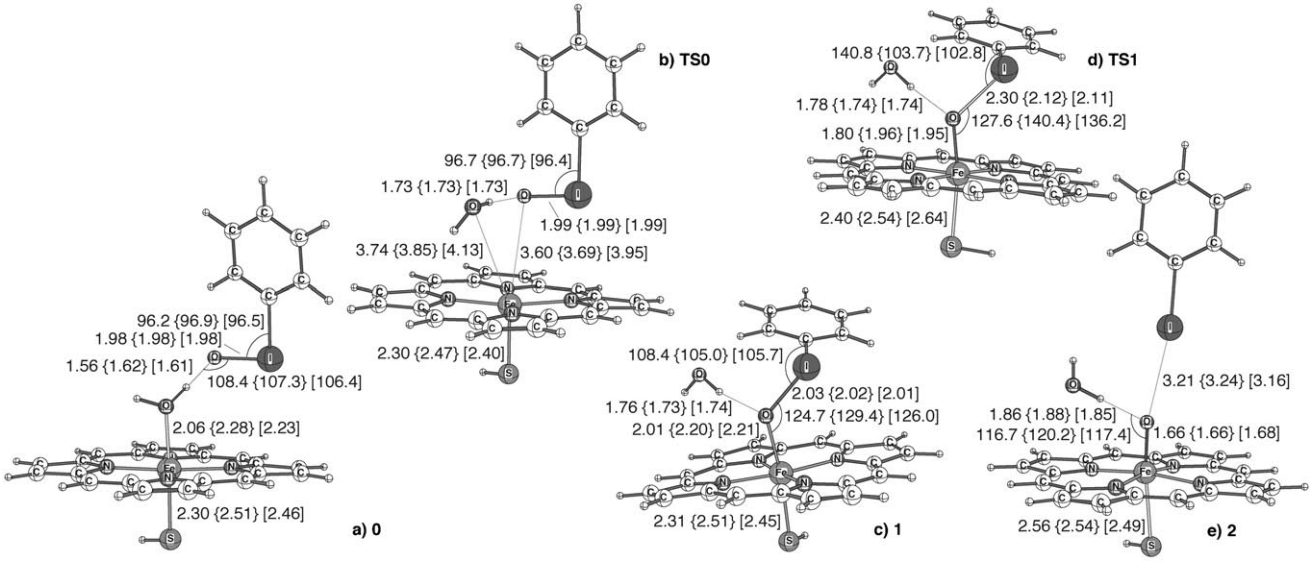

Figure 3. Optimized structure a) **0**, b) **TS0**, c) **1**, d) **TS1**, and e) **2** for reaction B. See legend of Figure 1 for explanation of the numbers.

The structures for **1** (Figure 3c), **TS1** (Figure 3d) and **2** (Figure 3e) in reaction B are largely as described for reaction A. Geometrically, the water is hydrogen bonded to the oxygen, and the only notable difference to reaction A is in **2**, in which the I–O distance is elongated by 0.1–0.2 Å; that is, the introduction of H_2O further weakens the I–O bond. Energetically, the internal energy changes (that is, the changes in the energy differences within each structure) are less than 1 kcal mol^{-1} with no internal order changes, with the sole exception of **2**, for which the difference between ^{4}**2** and ^{6}**2** drops from 9.1 to 7.6 kcal mol^{-1} and the order of preference changes between ^{2}**2** and ^{4}**2**. Looking at the changes of energy differences between the structures, once again **2** stands out by having their energies raised by 1.5–3.0 kcal mol^{-1}, reflecting the weaker I–O bond. Also here, relaxation of ^{6}**TS1** leads to the Fe–S bond break as described in reaction A.

For **TS1**, the barriers for different states remain close to each other as in reaction A. It can now be concluded that in the case of PhIO the crucial energy barrier in determining the final spin state of the product is the dislocation of water via **TS0**, due to the large energy difference between the doublet and the others, rather than **TS1**. The final energies for reaction B are shown in a graph in Figure 4.

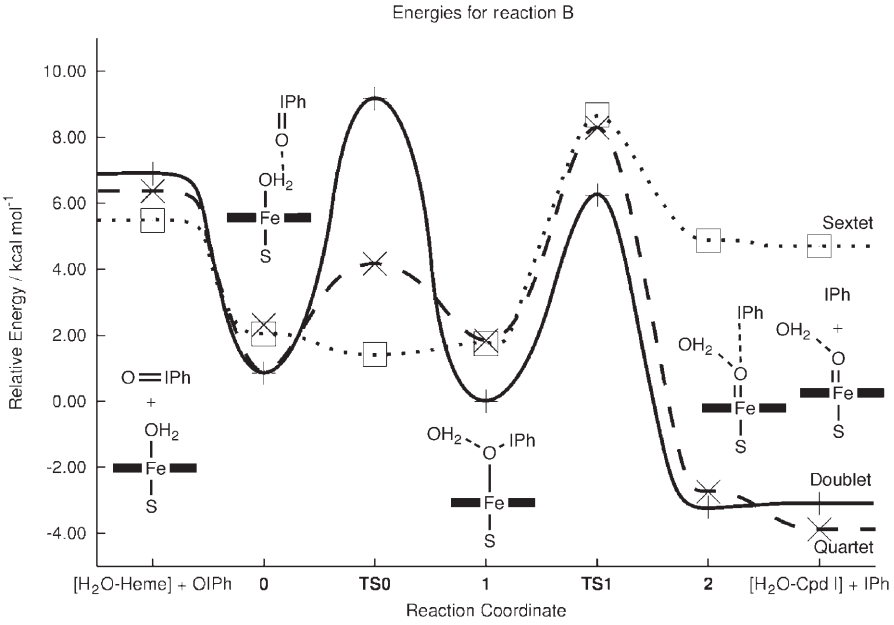

Figure 4. B3LYP energy profile for reaction B. The values are taken from Table 3.

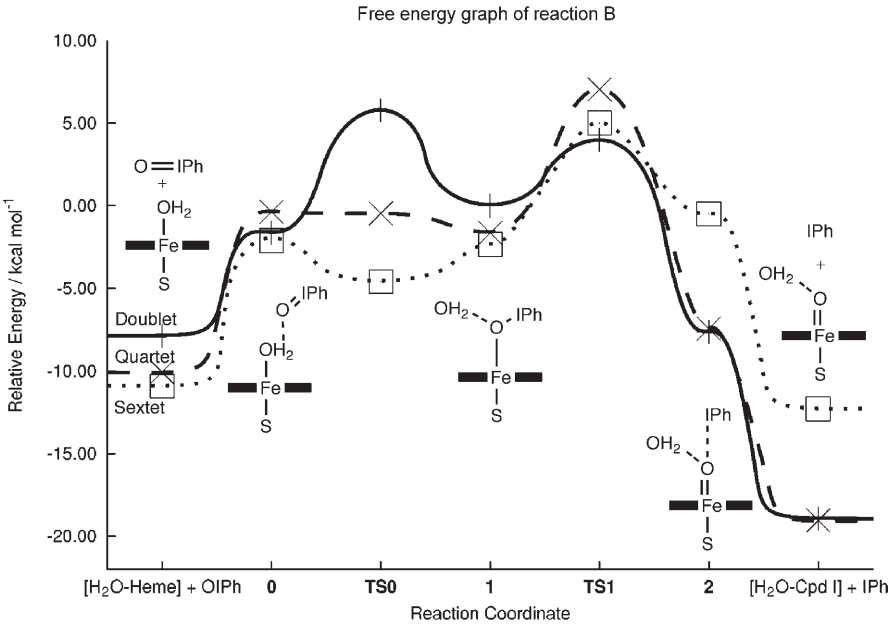

Figure 5. Free-energy profile for reaction B. The values are taken from Table S61.

Free energy changes for reaction B: It is instructive to consider also the free energy of this reaction (Figure 5). It should be stressed here that the endpoint free energies might not be reliable (resulting in large entropy effects due to the loss of translational and rotational degrees of freedom upon encounter). The free-energy comparisons from **0** to **2** are, however, reliable. The most interesting feature is that on the free-energy scale, the sextet surface is the lowest one for the range of structures **0**, **TS0**, and **1**. The quartet surface is also stabilized, ^{4}**1** being lower than ^{2}**1**. In addition, the gap between ^{2}**TS1** and ^{6}**TS1** is reduced from 2.4 to 1.0 kcal mol^{-1}, although the gap between ^{2}**TS1** and ^{4}**TS1** increases from 2.0 to 3.1 kcal mol^{-1}. Thus the inclusion of the thermal effects works favorably for the higher multiplicities with the sole exception of ^{4}**TS1**, something that is only reinforced if the sulfur ligand is hydrogen bonded as presented earlier.

Reaction C: Since the above results on reaction B indicate that the dislocation of water is independent of the oxygen donor, and that the presence of a water molecule does not

affect the subsequent step of Cpd I formation (see reaction A versus **1** to **2** in reaction B), we restricted the study of reaction C to the oxygen transfer from DMAO to the heme (Figure 6). In **1** (Figure 6a), DMAO is bound to heme in a similar manner as in reaction A. Also here, the lowest energy state is a doublet state, although the differences to the other states are within 1.4 kcal mol^{-1} (Table 4). However,

Table 4. Relative energies[a] for the different structures in reaction C [data in kcal mol^{-1}].

	Heme +DMAO	**1**	**TS1**	**2**	Cpd I +DMA
doublet	2.24	0.00	21.07	9.82	7.87
quartet	−1.96	1.41	28.10	9.37	8.09
sextet	−5.09	0.98	30.34	18.58	17.59

[a] Energies obtained as in Table 1.

the decisive difference to the PhIO reaction is seen in **TS1** (Figure 6b), which lies significantly higher in the case of DMAO. The energy barrier at **TS1**, while being in the range of 6.3–8.7 kcal mol^{-1} for PhIO (Table 3), is now in the range of 21.1–30.3 kcal mol^{-1} (Table 4), roughly four times higher. Furthermore, it can be seen in Table 4 that ^{2}**TS1** for reaction C is more than 7 kcal mol^{-1} lower than that for ^{4,6}**TS1**; hence the reaction will continue in a doublet state and produce a doublet product ^{2}**2** (Figure 6c). This confirms that unlike the PhIO case in which water dislocation makes the spin-state selection, for DMAO the oxygen-atom transfer process is the spin-selecting step. This high barrier in reaction C should provide ample time for spin relaxation at **1** from an initial high-spin heme, pentacoordinated state. According to earlier theoretical predictions,[40] this will generate a low KIE, as further documented in the next section.

The issue of the Fe–S bond breakage in the sextet state was found here too, with an extremely long Fe–S bond of 3.2 Å at the transition state ^{6}**TS1**. However, the energy landscape around this transition state was found to be relatively insensitive to the Fe–S bond length; it could vary down to 2.8 Å without significant energy changes. As in the case of PhIO, re-formation of the Fe–S bond was found to occur through a negligible barrier here as well (Figure S24 in the Supporting Information). We therefore present ^{6}**2** here as a structure in which the Fe–S bond is intact, in the same manner as in reactions A and B.

Theoretical KIE values for DMA hydroxylation by Cpd I: We calculate here the transition state (**TS$_H$**) of DMA hydroxylation by Cpd I in the doublet, quartet, and the sextet states from which we can calculate the energies and KIE. This would enable us to see whether the generation of Cpd I from PhIO versus DMAO may affect the spin-state selection. In addition to the doublet and quartet states, we found two possible electronic states for the sextet structure. One was a pentaradical state with valence electron orbitals $(\delta)^1(\pi^*_{xz})^1(\pi^*_{yz})^1(a_{2u})^1(\sigma^*_{xy})^1$, and the other a heptaradical state with the orbitals $(\delta)^1(\pi^*_{xz})^1(\pi^*_{yz})^1(a_{2u})^1(\sigma^*_{xy})^1(\sigma^*_{z^2})^1(\varphi_{subs})^1$, the last orbital being a spin-down orbital on the substrate. The heptaradical state was found to be lower in energy than the pentaradical state by 4.2 kcal mol^{-1} at the transition state, and features a long Fe–S distance of 3.3 Å, indicating that the Fe–S bond is broken. Comparisons with the doublet and quartet values are shown in Table 5.

The doublet and quartet KIE values are in line with earlier published values;[40] that is, low for the doublet and high for the quartet. Looking at the energy barriers for this step, both the sextet steps are high, with the pentaradical sextet state definitively ruled out. The 4.9 kcal mol^{-1} energy difference from the quartet also rules out the heptaradical sextet route, especially considering the efficient spin-orbit coupling between the sextet and quartet states,[41–43] which will serve to channel the sextet species to the quartet manifold. The doublet–quartet spin-orbit coupling is small, however, and

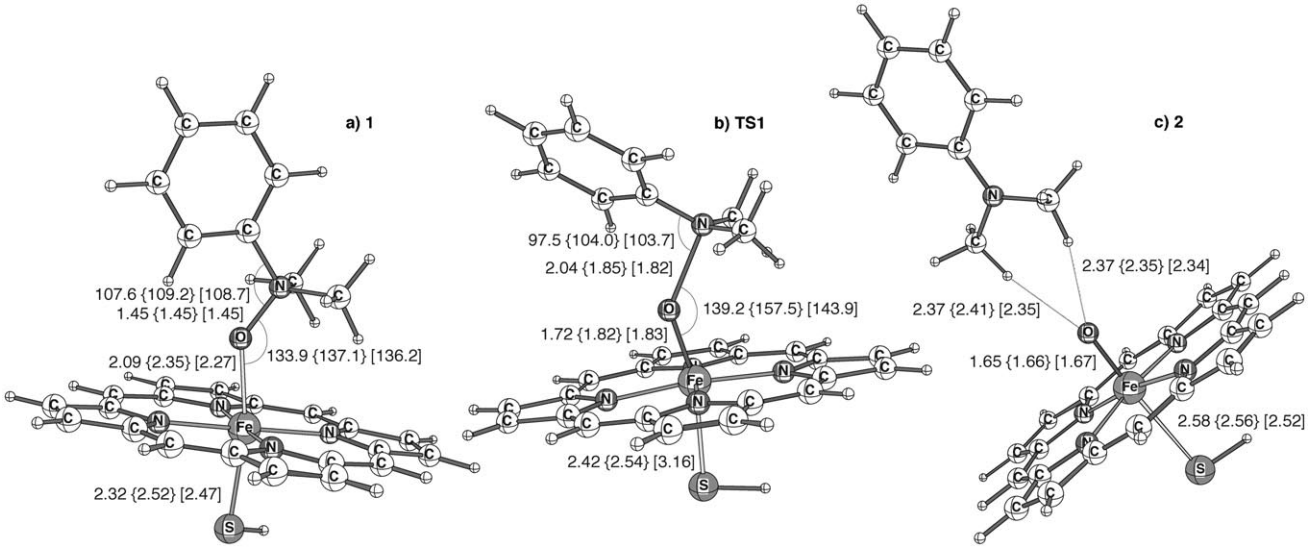

Figure 6. Optimized structures for reaction C. a) **1** b) **TS1**, and c) **2**. See legend of Figure 1 for explanation of the numbers.

Table 5. Theoretically calculated $\mathbf{TS_H}$ energies and average KIE values for hydrogen atom abstraction by ^{2,4,6}CpdI from deuterium substituted *N*,*N*-$(CD_2H)_2$-aniline at $T = 298.15$ K.[a]

	Doublet	Quartet	Sextet[e]	Sextet[f]
KIE1[b]	3.79	5.78	5.59	2.34
KIE2[c]	4.06	7.75	7.53	2.34
energy[d]	6.44	8.78	17.95	13.72

[a] Note that experimental KIEs in reference [24] and here are at $T = 310$ K. [b] Eyring model. [c] Wigner correction with scaled frequency by scale factor 0.9704. [d] Energy in kcal mol^{-1} relative to ^{4}**2** in reaction C. [e] Pentaradical. [f] Heptaradical.

with such a small doublet–quartet energy difference as 2.3 kcal mol^{-1}, the quartet barrier should be small enough to allow reactions to continue in the quartet state given favorable conditions. It has been suggested earlier that this difference in the spin states may give rise to different KIE values,[40] and applied to the current case, the KIE jump observed when using PhIO-generated CpdI may be due to the reactions occurring in the quartet state (see Discussion below). Since the calculations show that on the sextet surface the thiolate may be detached for the porphyrin–iron–oxo moiety (PorFeO) during the formation of CpdI, we have also considered the hydroxylation of the DMA by PorFeO devoid of the SH ligand. These results are presented in Supporting Information (Part 4).

Experimental determination of KIE for *N*,*N*-dimethyl-4-(methylthio)aniline dealkylation: Guengerich et al.[24] reported that the KIE for N-dealkylation of *N*,*N*-dimethylaniline was 1.7 and 6.7 for dealkylation of *N*-methyl-*N*-(trideuteromethyl)aniline by the native route and with PhIO, respectively. Since KIE values for *N*-methyl-*N*-(trideuteromethyl)aniline have been determined to be masked and give smaller KIE values for some P450 enzymes than when *N*,*N*-bis(dideuteromethyl-^{13}C)aniline is used to determine the isotope effect,[30] we decided to test the KIE jump using this more sophisticated experimental design. Thus, the experimental KIE was determined for the N-dealkylation of *N*,*N*-dimethyl-^{13}C-4-(methylthio)aniline to ascertain if the KIE jump observed by Guengerich et al.[24] for PhIO with respect to the native route could be reproduced, or if it was a result of differences in the masking of the intrinsic isotope effect for the two systems. A KIE jump was also observed for *N*,*N*-dimethyl-^{13}C-4-(methylthio)aniline, which gave a KIE of 2.2 for the NADPH/O_2/P450 system and a KIE of 4.2 for the PhIO-supported system, confirming that the KIE differences are not a result of differing kinetics, but instead reflect a change in transition-state structure. It is important to recognize that intramolecular KIE values reported here are free of masking from other rate-limiting steps ("kinetic complexity"). This has been shown by using a detailed kinetics model[44] and a number of arguments further support this statement:

1) The KIEs determined for substituted anilines in the native P450 system are the same in six different P450 enzymes; this would require every enzyme to show the same amount of masking, which is not too probable.[45]
2) The native P450 system gives identical KIEs as the enzyme in which CpdI is generated by using DMAO analogues as the oxygen donor; this identity of the KIEs is inconsistent with masking effects in the native enzyme, since the rate-limiting steps are different in these two systems.[11]
3) In a series of *N*,*N*-dimethylanilines, the changes in intramolecular KIEs reflect a change in reaction energies consistent with the Melander–Westheimer postulate and inconsistent with masking.[11]

Thus, our KIE data above for the native route and the PhIO routes are reliable data free of kinetic complexities. As such, the observation of Guengerich et al.[24] carries over to another substrate, showing that the use of PhIO leads to a higher KIE value, which can be as high as 6–7 for DMA itself.

Discussion

Our theoretical results show that while PhIO will generate CpdI in its higher spin multiplicities due to water dislocation barriers (Table 3), N–O surrogates such as DMAO will generate the species exclusively in its doublet state due to oxygen-transfer barriers (Table 4). As outlined below, these results can provide a consistent rationale for experimental observations of the KIE jump in the PhIO route, compared with the constant KIE in the DMAO route. Figure 7 shows the computational scenario for the generation of CpdI from a DMAO surrogate followed by the hydrogen abstraction from DMA.

As we argued in the results section, the water dislocation step from the resting state will be identical for different oxygen surrogates. Therefore, we start the DMAO reaction at **TS0**; the data for **TS0** was taken from reaction B (modified with respect to different oxygen–heme binding energies). Following the release of water, which has relatively low barriers compared with those in the rate-determining step for this surrogate, complex C**1** (Figure 7) has to surmount a very high barrier, to transfer the oxygen from the N–oxo moiety of DMAO to the iron and generate CpdI, followed by much smaller barriers for hydrogen abstraction. Since the oxygen-transfer barrier via ^{2}**TS1** is the lowest (by 7.0 and 9.2 kcal mol^{-1}, compared with the other states), the reaction will proceed selectively from the doublet state, thereby forming doublet CpdI. This will be followed by a very fast step of hydrogen abstraction from DMA, which again has the lowest barrier on the doublet surface, via $^2\mathbf{TS_H}$. Therefore, CpdI will perform mostly a doublet state reaction when formed from DMAO. Furthermore, it follows that CpdI prepared in the native route will also perform hydrogen abstraction mostly via $^2\mathbf{TS_H}$, even if ^{2}CpdI and ^{4}CpdI undergo spin equilibration, since the $^2\mathbf{TS_H}$ species is lower than $^4\mathbf{TS_H}$. For this reason, the experimental KIE

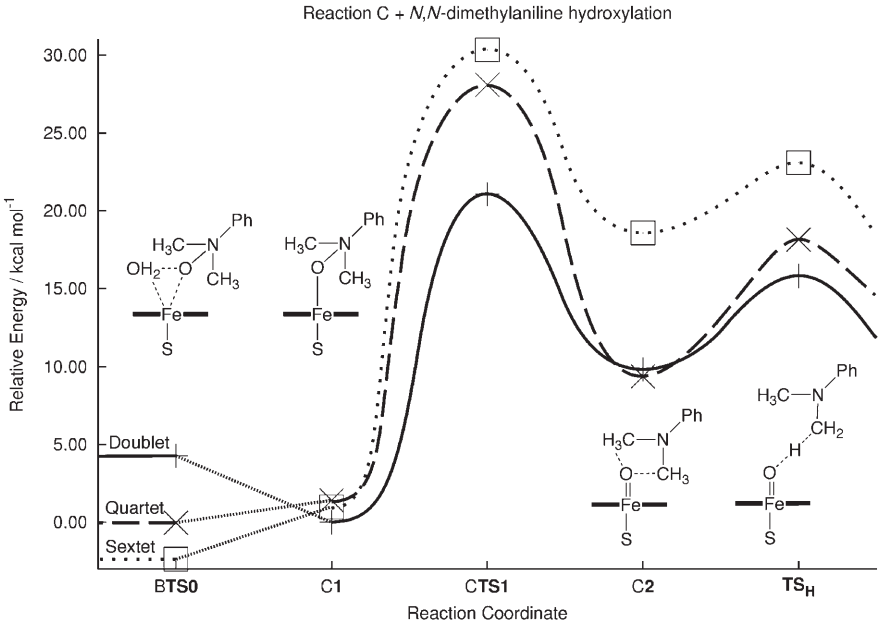

Figure 7. Full energy profile from heme resting state with DMAO to CpdI followed by H-abstraction from DMA. The water dislocation **TS0** of reaction B has been patched to reaction C, in which the relative energies of **TS0** have been adjusted accounting for the different oxygen-donor binding energy to heme according to Tables 1 and 4. At the end, the energy profile results for DMA hydroxylation have been added to reaction C. The reaction coordinate axis labels starting with "B" or "C" refer to the reactions B or C, respectively. The exact values for this graph are found in Table S85.

values measured in the process in which CpdI is nascent from the N–O surrogate are virtually identical to the ones measure from the native process of the enzyme, using NADPH and O_2.[11] Both sets of the measured KIE values are low for the entire series of *N*,*N*-dimethylanilines, in agreement with the theoretical prediction that the doublet state leads to a low KIE value. Thus, the calculated barrier scenario and KIE values lead to the same conclusion that the use of the N–O surrogate results in a selective doublet-state reaction.

The corresponding scenario for PhIO is depicted in Figure 8 and is seen to be entirely different than the case of DMAO. Here the water dislocation step is rate limiting for the doublet state. The corresponding barrier (via **TS0**) is 5.0 kcal mol^{-1} higher than the quartet and 7.8 kcal mol^{-1} higher than the sextet (Table 3). Therefore, this barrier could act as a filter that produces preferentially quartet and sextet species of the Fe-O-IPh complex, **1** (B**1** in Figure 8). In the absence of water as a ligand the ^{6}**1** species is produced directly from the ground state of the pentacoordinate complex (Figure 2 and Table S28). An analogous sextet-state complex (devoid of a proximal ligand to the iron) was identified by Nam et al,[28] based on changes in UV/VIS, EPR, and X-ray absorption spectra. As can be further seen from Figure 8, during the formation of CpdI (B**2**) the quartet surface goes down in energy, while the sextet state rises high. Since the quartet and sextet states of **1** and **TS1** maintain strong spin-orbit coupling,[41–43] the most likely outcome of this scenario is a spin flip from the sextet to the quartet, to generate CpdI in its quartet state. Since at this stage the spin-orbit coupling between the quartet and doublet states is small, the quartet state can then abstract a hydrogen atom from DMA via ^{4}**TS$_H$** before spin flip to a doublet state can occur. Thus, the KIE for the PhIO-supported hydroxylation process will correspond to the quartet-state

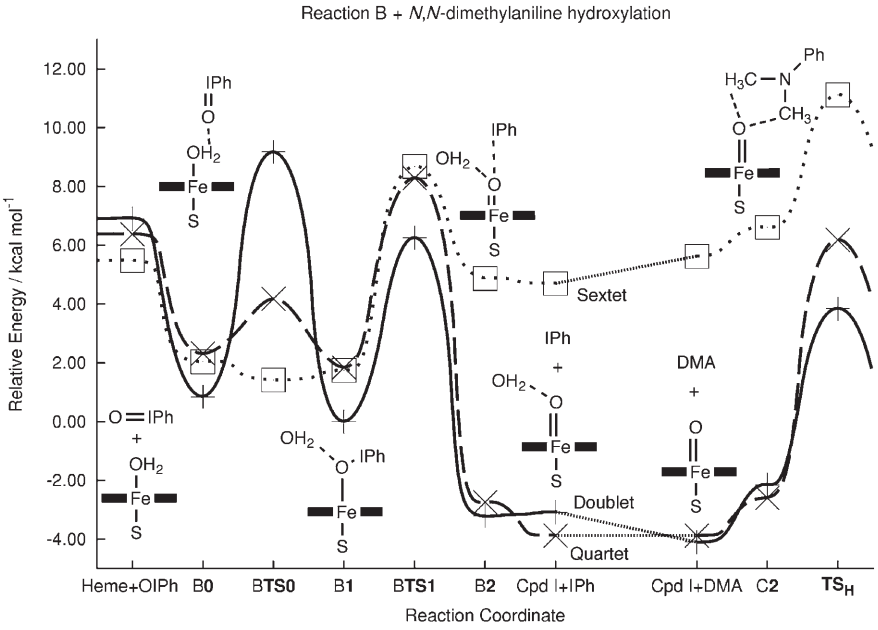

Figure 8. Full energy profile from heme resting state with PhIO to CpdI followed by hydrogen abstraction from DMA. Reaction B has been patched at CpdI+IPh stage with the profiles for CpdI+DMA results. The reaction coordinate axis labels starting with "B" or "C" refer to the reactions B or C, respectively. The exact values for this graph are found in Table S62.

process. It follows therefore that, the N-dealkylation reaction of DMA may occur through different spin states under different conditions (native, N−O or PhI=O route).

As already mentioned, the KIE of the native route is low. The N-dealkylation of DMA in $P450_{2B1}$ has been experimentally shown to occur with a KIE of 2.5,[45] while the PhIO-supported reaction yields a KIE of 6.7.[24] We confirmed experimentally in this study that a larger KIE is observed for *N*-dealkylation reactions with another substrate, *N*,*N*-dimethyl-4-(methylthio)aniline, and a different enzyme, $P450_{BM3}$, when the NADPH/O_2-supported reaction is compared to that of PhIO (2.2 versus 4.2, respectively). The theoretically calculated KIE values for the doublet and quartet states fit these values (Table 5); the doublet state leads to a low value (3.79/4.06), while the quartet state leads to a high one (5.78/7.75).

The scenario described above for the PhIO-supported reaction versus the native process provides a logical explanation for a very enigmatic experimental result. What strengthens and lends credibility to this scenario is the contrasting outcome using the N−O oxygen surrogate. Indeed, here for the same substrate, *N*,*N*-dimethyl-4-(cyano)aniline, as well as others,[11] the KIE values obtained using the N−O surrogate and the native route are now virtually identical and low. Thus, the theoretical data in terms of energetics and KIE scenarios of the processes for the two oxygen surrogates match experimental results and provide a unified description for the two sets of data. Other scenarios (e.g., the thiolate dissociation scenario) that were considered and discarded are given in full in the Supporting Information.

A key element in the scenario is the reactivity of the substrate undergoing hydroxylation. Thus, fast-reacting substrates like DMA[24] or *N*,*N*-dimethyl-4-(methylthio)aniline (as shown in the present study) exhibit a jump when the Cpd I species is generated with PhIO relative to the values obtained in the "native route" (O_2/NADPH) of the enzyme. However, for slow reactions (i.e. high $^{2,4}\mathbf{TS_H}$ with close-lying spin states) such as allylic oxidation of cyclohexene, the spin states will have sufficient time to equilibrate and the KIE values should always correspond to two-state reactivity of Cpd I. In most of the cases with less reactive C−H bonds, the KIE(doublet) and KIE(quartet) values are both high and quite close to each other (KIE(doublet) ≈ KIE(quartet)).[37,46] Indeed, virtually identical KIE values have been measured when either cumene hydroperoxide or NADPH/O_2 are used for cyclohexene,[47] and Gelb et al.[48] found that PhIO-supported hydrogen-atom abstractions with $P450_{cam}$ gave identical isotope ratios as the NADPH/O_2-supported reaction of camphor. Scheme 2 shows a summarized view of these conclusions, and Table 6 collects known experimental KIE values for comparisons.

The relative energies are, as we have shown here, subject to additional factors such as hydrogen bonds and entropy effects, among others. Therefore, few kcal mol^{-1} variations in the relative energies are expected, and one should be careful drawing conclusions based on close-lying differences. In this study, however, the main conclusions derive from two large differences that should be outside any error margins: one is the **TS0** water-displacing step, in which the doublet–sextet energy difference is 7.8 kcal mol^{-1}, and **TS1** in reaction C, in which the doublet–quartet difference is 7.0 kcal mol^{-1}. This coupled to the small doublet–quartet energy difference in $\mathbf{TS_H}$ (2.3 kcal mol^{-1}) should enable the hydroxylation reaction to proceed in either spin state, as determined by the preceding barriers. This is one possible, simple interpretation of our current data, in an attempt to explain the measured KIE differences in what is likely to be a complicated reaction. As with all theoretical model calculations, however, this may be in need of further experimental verifications. Furthermore, a sober note of caution is necessary to emphasize that our study did not rule out the possibility that **1** will undergo protonation on the oxo group, which upon release

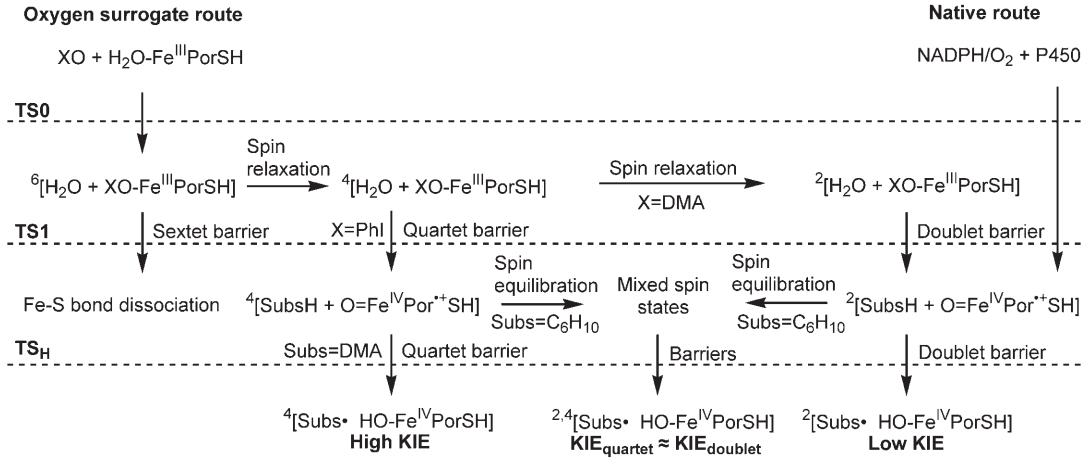

Scheme 2. Possible pathways of induced Cpd I by the oxygen surrogate route (XO = PhIO/DMAO) versus the native route (NADPH/O_2). The labels **TS0**, **TS1**, and $\mathbf{TS_H}$ correspond to the transition states of water dislocation, Cpd I formation, and hydrogen abstraction from the substrate, respectively (see text). For the oxygen surrogate route, passing the **TS0** barrier generates a sextet; spin relaxation will allow the complex to pass **TS1** as a doublet or quartet to form ^{2,4}Cpd I. The final predicted KIE ranges depend on the spin state of the complex when passing $\mathbf{TS_H}$, and are shown in bold. Left-hand superscripts denote system spin multiplicity.

Table 6. Experimental KIE values.

Substrate	Enzyme	Oxygen donor	KIE	Reference
DMA and/or analogues	$P450_{cam}$	$NADPH/O_2$	2.23–3.1	[11]
	$P450_{cam}$	DMAO analogues	2.53–3.07	[11]
	$P450_{2E1}$	$NADPH/O_2$	2.92–3.65	[11]
	$P450_{2E1}$	DMAO analogues	2.87–3.66	[11]
	$P450_{2B1}$	$NADPH/O_2$	1.56–3.56	[24]
	$P450_{2B1}$	PhIO	6.7–7.3	[24]
	Porphine[a]	DMAO	3.79/4.06	this study
	Porphine[a]	PhIO	5.78/7.75	this study
	$P450_{BM3}$	$NADPH/O_2$	2.2	this study
	$P450_{BM3}$	PhIO	4.2	this study
	6 P450 species	$NADPH/O_2$	2.4–4.1	[45]
cyclohexene[b]	$P450_{LM2}$	$NADPH/O_2$	4.1–4.9	[47]
	$P450_{LM2}$	Cum-OOH	4.8–5.1	[47]
camphor[c]	$P450_{cam}$	$NADPH/O_2$	1.18/4.51/4.39	[48]
	$P450_{cam}$	PhIO	1.48/3.76/4.69	[48]

[a] Theoretical model used in this study with calculated Eyring/Wigner KIE values assigned to DMAO and PhIO supported reactions according to the Discussion section. [b] Cum-OOH is cumeme peroxide. The values varied slightly depending on the equation used. [c] These three sets are hydrogen/deuterium isotope ratios in the product alcohol but are not KIE values. The values were measured where the camphor was deuterized at 5-*exo*/5,6-*endo*/5-*endo* positions.

of PhI, will give rise to a protonated Cpd I species that leads to substrate oxidation. This would, however, require the observation of KIE jumps/variation, compared with the native route, for all substrates; something which is not observed.

Conclusion

In conclusion, it is clear that the seemingly simple reaction in Scheme 1 becomes intriguingly complex due to the different available spin states, and the energetics may very well be sensitive to the kind of systems used, both for the porphyrin and the oxygen donor, as has been found experimentally.[26–29] Nevertheless, the present study at least shows that the existence of a PhIO–heme complexed system **1** is indeed possible, and so is the incursion of **2**, the PhI–Cpd I complex. However, the weakness of the complexation interaction between PhIO and the Fe(Por) in **1** and between PhI and Cpd I in **2** casts doubts on the suggestions that, for example, **2** is the root cause of the differences in the reactivity between the native route and the PhIO route. While a protonated Cpd I generated from **1** cannot be ruled out, it remains unclear how such a species can explain the KIE jump that is observed in DMA and similar substrates but not in others.

At the same time, our results regarding the importance of different spin states provide a reasonable explanation, hitherto unconsidered, for the observed experimental KIE jumps. In the case of PhIO, the energy barrier of going from **1** to **2** is only marginal for the higher spin states (Figure 8). This makes it possible that ^{4}Cpd I could be the oxidizing species, at least for a finite time before relaxing to a doublet, hence giving a high KIE. Moreover, the calculations also show that DMAO-supported Cpd I formation should occur exclusively on the doublet surface (Figure 7), consistent with available experiments showing low KIE for this reaction.[11] The KIE jump observed here experimentally for *N*,*N*-dimethyl-4-(methylthio)aniline when using PhIO compared with the native route, and the identical KIE for the N–O route and the native route for the same substrate (and others) further support the theoretical model. In our view, this correlation between the spin states and measured KIE is not coincidental. However, the general applicability of this requires an extensive systematic investigation of theory and experiment involving a variety of oxygen surrogates.

Experimental Section

Computational methods: All the calculations were done with the density functional theory (DFT) formalism[49] by using the B3LYP hybrid functional.[50–53] Even though there is criticism on the accuracy of B3LYP for reproducing spin-state ordering, there is ample evidence that it is reliable for heme complexes of the type studied here. As has been shown for Cpd I,[35] the UB3LYP spin state ordering is in good agreement with the results of extensive configuration interaction calculations. More relevant evidence is provided in the Supporting Information. Ground-state geometry optimizations were done with Jaguar 5.5,[54] while transition state optimizations and frequency calculations were done by Gaussian 03.[55] The basis set used here was LACVP, a basis set of double-ζ quality with an effective core potential (ECP) on iron, as defined in Jaguar. Single-point solvent and larger basis set calculations were done on the LACVP-optimized geometries with Jaguar. In the solvent calculations, the dielectric constant of $\varepsilon = 5.71$ and the probe molecule radius of 2.721 Å was used, corresponding to chlorobenzene. Calculations with a large basis set used ERMLER2^{*+} on iodine[56,57] and LACV3P^{*+} on the rest (corresponding to LACV3P^{+} on Fe), to obtain more accurate energies (see below). The ERMLER2^{*+} basis set involves, on iodine, a small core relativistic ECP with scalar and spin orbit correction. In the Jaguar implementation, the 4d, 5s, and 5p valence shells are outside of the core.[56] The basis set is of double-ζ quality augmented with diffuse and polarization functions taken from the relativistic all-electron double-ζ basis set of Dyall.[57]

Basis-set calibration: Since two of our reactions included the heavy atom iodine, it was necessary to validate the use of our usual protocol LACV3P^{*+}//LACVP, especially since in the case of iodine the LACV3P^{*+} basis set is per definition the same as LAV3P in Jaguar. To this end, comparisons were made with the basis set ERMLER2^{*+} as implemented in Jaguar. In the first test suite, the I_2 dissociation energy was used as a benchmark system. Here, LACV3P^{*+} yielded an I_2 bond energy of 60.7 kcal mol^{-1}, while the single-point ERMLER2^{*+} yielded 21.4 kcal mol^{-1}. Experimental values put the energy at 36.1 kcal mol^{-1}.[58] The large discrepancy, with experiment, was in part due to the poor optimized geometry produced by LACVP. Looking at the structure, the calculated bond length was at 3.37 Å, compared to 2.70 Å found experimentally. Indeed, optimizing I_2 using ERMLER2^{*+} instead yielded a bond length of 2.78 Å, and a much more accurate bond dissociation energy value of 39.5 kcal mol^{-1}. Thus, LACVP yields an extremely poor geometry in the case of I_2, whereas ERMLER2^{*+} proved to be a reliable basis set for iodine, both with regards to the geometry and the energy of I_2. Another benchmark test was then performed, this time on the IO$^{\bullet}$ radical. Optimization with LACVP and subsequent single-point calculation with LACV3P^{*+} yielded a bond energy of 46.1 kcal mol^{-1}. Replacing the

basis set on I with ERMLER2*+ in a single-point calculation gives 53.5 kcal mol^{-1}. Re-optimizing the structure with the latter basis set combination changed only slightly the bond length from 2.01 to 1.95 Å and the bond dissociation energy to 54.4 kcal mol^{-1}. Available experimental values put this energy to 59.5 kcal mol^{-1}.[58] Thus the geometry was accurately treated with LACVP, but a more than 7 kcal mol^{-1} energy discrepancy between LACV3P*+ with ERMLER2*+ was still apparent in the bond dissociation energies. The discrepancy was worse when the I–O bond strength was examined in PhIO, for which LACV3P*+ gave a bond strength of 13.3 kcal mol^{-1}, but single-point ERMLER2*+ gave 27.3 kcal mol^{-1}. However, geometry optimizations with ERMLER2*+ on iodine and LACV3P*+ on the rest of the atoms changed the relevant geometries by less than 0.1 Å (and the bond-energy difference less than 2 kcal mol^{-1} compared to the single point), confirming that the geometry was sufficiently reproduced at LACVP level. The selected procedure employed therefore LACVP for optimization, and the LACV3P*+ basis set in combination with ERMLER2*+ on iodine (when present) for the single-point energy evaluation.

Theoretical KIE calculations: KIE calculations were carried out for the reaction of DMA hydroxylation with Cpd I, following established procedures.[46] Since calculations indicated that during the formation of Cpd I in the sextet state the Fe–S bond may dissociate, we deemed it necessary to explore also the KIE results with the thiolate ligand-free Cpd I, in order to ascertain the consistency of the conclusions (see the Supporting Information).

Experimental KIE measurements: Intramolecular KIE values were determined for the N-dealkylation of *N,N*-dimethyl-4-(methylthio)aniline as described by Volz et al.[59] For enzymatic incubations, 10 mL scintillation vials were charged with substrate (1.6 μmol in 9 μL methanol), purified $P450_{BM3}$ enzyme (200 pmol), glucose-6-phosphate (9.2 μmol), glucose-6-phosphate dehydrogenase (0.40 nmol), catalase (0.34 nmol), and magnesium chloride (4.2 μmol) in phosphate buffer (0.1 M, pH 7.4) to give a total volume of 990 μL. The incubations were initiated by adding NADP (1.2 μmol in 110 μL of the phosphate buffer) and placed in a shaker bath at 30°C for 25 min. The incubations were terminated by adding methanol (300 μL) and filtered through a 0.45 μm filter. Enzymatic products were analyzed by liquid chromatography mass spectrometry (LC-MS) using electrospray ionization as described by Dowers et al.[11] For the PhIO-supported reactions the glucose-6-phosphate, glucose-6-phosphate dehydrogenase, and NADP were left out of the reaction and PhIO was added to a final concentration of 2 mM.

Acknowledgements

S.S. acknowledges support by the German Federal Ministry of Education and Research (BMBF) within the framework of the German–Israeli Project Cooperation (DIP) and by the Israel Science foundation (ISF). J.P.J. acknowledges the National Institute of Environmental and Health Sciences Grant 09122.

[1] G. H. Loew, D. L. Harris, *Chem. Rev.* **2000**, *100*, 407–419.
[2] B. M. Meunier, S. P. de Visser, S. Shaik, *Chem. Rev.* **2004**, *104*, 3947–3980.
[3] P. R. Ortiz de Montellano in *Cytochrome P450, 3rd ed.* (Ed.: P. R. Ortiz de Montellano), Kluwer Academic/Plenum, New York, **2005**.
[4] T. Spolitak, J. H. Dawson, D. P. Ballou, *J. Biol. Chem.* **2005**, *280*, 20300–20309.
[5] M. Newcomb, R. Zhang, R. E. P. Chandrasena, J. A. Halgrimson, J. H. Horner, T. M. Makris, S. G. Sligar, *J. Am. Chem. Soc.* **2006**, *128*, 4580–4581.
[6] E. G. Hrycay, J.-Å. Gustafsson, M. Ingelman-Sundberg, L. Ernster, *FEBS Lett.* **1975**, *56*, 161–165.
[7] E. G. Hrycay, J.-Å. Gustafsson, M. Ingelman-Sundberg, L. Ernster, *Biochem. Biophys. Res. Commun.* **1975**, *66*, 209–216.
[8] A. Berg, K. Carlström, J.-Å. Gustafsson, M. Ingelman-Sundberg, *Biochem. Biophys. Res. Commun.* **1975**, *66*, 1414–1423.
[9] F. Lichtenberger, W. Nastainczyk, V. Ullrich, *Biochem. Biophys. Res. Commun.* **1976**, *70*, 939–946.
[10] J.-Å. Gustafsson, J. Bergman, *FEBS Lett.* **1976**, *70*, 276–280.
[11] T. S. Dowers, D. A. Rock, J. P. Jones, *J. Am. Chem. Soc.* **2004**, *126*, 8868–8869.
[12] R. C. Blake II, M. J. Coon, *J. Biol. Chem.* **1989**, *264*, 3694–3701.
[13] J.-Å. Gustafsson, L. Rondahl, J. Bergman, *Biochemistry* **1979**, *18*, 865–870.
[14] U. M. Kent, S. Yanev, P. F. Hollenberg, *Chem. Res. Toxicol.* **1999**, *12*, 317–322.
[15] U. M. Kent, E. S. Roberts-Kirchhoff, N. Moon, W. R. Dunham, P. F. Hollenberg, *Biochemistry* **2001**, *40*, 7253–7261.
[16] A. D. N. Vaz, E. A. Roberts, M. J. Coon, *J. Am. Chem. Soc.* **1991**, *113*, 5886–5887.
[17] F. P. Guengerich, A. D. N. Vaz, G. N. Raner, S. J. Pernecky, M. J. Coon, *Mol. Pharmacol.* **1997**, *51*, 147–151.
[18] M. N. Bhakta, P. F. Hollenberg, K. Wimalasena, *J. Am. Chem. Soc.* **2005**, *127*, 1376–1377.
[19] M. Newcomb, P. H. Toy, *Acc. Chem. Res.* **2000**, *33*, 449–455.
[20] T. L. Macdonald, W. G. Gutheim, R. B. Martin, F. P. Guengerich, *Biochemistry* **1989**, *28*, 2071–2077.
[21] S. Modi, D. E. Gilham, M. J. Sutcliffe, L.-Y. Lian, W. U. Primrose, C. R. Wolf, G. C. K. Roberts, *Biochemistry* **1997**, *36*, 4461–4470.
[22] X. Shan, L. Que, Jr. *J. Inorg. Biochem.* **2006**, *100*, 421–433.
[23] A. Berg, M. Ingelman-Sundberg, J.-Å. Gustafsson, *J. Biol. Chem.* **1979**, *254*, 5264–5271.
[24] F. P. Guengerich, C.-H. Yun, T. L. Macdonald, *J. Biol. Chem.* **1996**, *271*, 27321–27329.
[25] P. R. Ortiz de Montellano in *Cytochrome P450, 1st ed.* (Ed.: P. R. Ortiz de Montellano), Plenum, New York, **1987**, pp. 217–271.
[26] J. P. Collman, A. S. Chien, T. A. Eberspacher, J. I. Brauman, *J. Am. Chem. Soc.* **2000**, *122*, 11098–11100.
[27] J. P. Collman, L. Zeng, R. A. Decréau, *Chem. Commun.* **2003**, 2974–2975.
[28] W. Nam, S. K. Choi, M. H. Lim, J. U. Rohde, I. Kim, J. Kim, C. Kim, L. Que Jr, *Angew. Chem.* **2003**, *115*, 113–115; *Angew. Chem. Int. Ed.* **2003**, *42*, 109–111.
[29] For the use of PhIO in nonheme complexes, see: Y. Suh, M. S. Seo, K. M. Kim, Y. S. Kim, H. G. Jang, T. Tosha, T. Kitagawa, J. Kim, W. Nam, *J. Inorg. Biochem.* **2006**, *100*, 627–633.
[30] J. P. Dinnocenzo, S. B. Karki, J. P. Jones, *J. Am. Chem. Soc.* **1993**, *115*, 7111–7116.
[31] F. Ogliaro, S. P. de Visser, S. Shaik, *J. Inorg. Biochem.* **2002**, *91*, 554–567.
[32] P. Rydberg, E. Sigfridsson, U. Ryde, *J. Biol. Inorg. Chem.* **2004**, *9*, 203–223.
[33] A. Altun, W. Thiel, *J. Phys. Chem. B* **2005**, *109*, 1268–1280.
[34] F. Ogliaro, S. P. de Visser, J. T. Groves, S. Shaik, *Angew. Chem.* **2001**, *113*, 3612–3612; *Angew. Chem. Int. Ed.* **2001**, *40*, 2874–2878; .
[35] J. Schöneboom, F. Neese, W. Thiel, *J. Am. Chem. Soc.* **2005**, *127*, 5840–5853.
[36] F. Ogliaro, S. Cohen, S. P. de Visser, S. Shaik, *J. Am. Chem. Soc.* **2000**, *122*, 12892–12893.
[37] H. Hirao, D. Kumar, W. Thiel, S. Shaik, *J. Am. Chem. Soc.* **2005**, *127*, 13007–13018.
[38] J. Schöneboom, W. Thiel, *J. Phys. Chem. B*, **2004**, *108*, 7468–7478.
[39] S. Shaik, D. Kumar, S. P. de Visser, A. Altun, W. Thiel, *Chem. Rev.* **2005**, *105*, 2279–2328.
[40] C. Li, W. Wu, D. Kumar, S. Shaik, *J. Am. Chem. Soc.* **2006**, *128*, 394–395.
[41] D. Danovich, S. Shaik, *J. Am. Chem. Soc.* **1997**, *119*, 1773–1786.
[42] Y. Shiota, K. Yoshizawa, *J. Chem. Phys.* **2003**, *118*, 5872–5879.
[43] Going from quartet to sextet in Cpd I involves a shift of an electron from the doubly occupied $\delta_{x^2-y^2}$ to the σ^*_{xy} orbital, the latter is delocalized over the iron and the nitrogen atoms of the heme. Such delocalization will reduce the spin-orbital coupling, although the value may still be high enough to induce fast spin inversion. The spin-orbit coupling between the quartet and doublet states is much less

efficient, since the two states differ simply by the direction of the spin in the a_{2u} orbital of the porphyrin.
[44] L. Higgins, G. A. Bennett, M. Shimoji, J. P. Jones, *Biochemistry*, **1998**, *37*, 7039–7046.
[45] S. B. Karki, J. P. Dinnocenzo, J. P. Jones, K. R. Korzekwa, *J. Am. Chem. Soc.* **1995**, *117*, 3657–3664.
[46] D. Kumar, S. P. de Visser, P. K. Sharma, S. Cohen, S. Shaik, *J. Am. Chem. Soc.* **2004**, *126*, 1907–1920.
[47] J. Groves, *Adv. Chem. Ser.* **1980**, *191*, 227–289.
[48] M. H. Gelb, D. C. Heimbrook, P. Malkonen, S. G. Sligar, *Biochemistry* **1982**, *21*, 370–377.
[49] W. Kohn, L. J. Sham, *Phys. Rev. A* **1965**, *140*, 1133–1138.
[50] A. D. Becke, *Phys. Rev. A* **1988**, *38*, 3098–3100.
[51] A. D. Becke, *J. Chem. Phys.* **1993**, *98*, 1372–1377.
[52] A. D. Becke, *J. Chem. Phys.* **1993**, *98*, 5648–5652.
[53] C. Lee, W. Yang, R. G. Parr, *Phys. Rev. B* **1988**, *37*, 785–789.
[54] Jaguar 5.5, Schrodinger, LLC, Portland, OR (USA), **2003**.
[55] Gaussian 03, Revision B.05, M. J. Frisch, G. W. Trucks, H. B. Schlegel, G. E. Scuseria, M. A. Robb, J. R. Cheeseman, J. A. Montgomery, Jr., T. Vreven, K. N. Kudin, J. C. Burant, J. M. Millam, S. S. Iyengar, J. Tomasi, V. Barone, B. Mennucci, M. Cossi, G. Scalmani, N. Rega, G. A. Petersson, H. Nakatsuji, M. Hada, M. Ehara, K. Toyota, R. Fukuda, J. Hasegawa, M. Ishida, T. Nakajima, Y. Honda, O. Kitao, H. Nakai, M. Klene, X. Li, J. E. Knox, H. P. Hratchian, J. B. Cross, V. Bakken, C. Adamo, J. Jaramillo, R. Gomperts, R. E. Stratmann, O. Yazyev, A. J. Austin, R. Cammi, C. Pomelli, J. W. Ochterski, P. Y. Ayala, K. Morokuma, G. A. Voth, P. Salvador, J. J. Dannenberg, V. G. Zakrzewski, S. Dapprich, A. D. Daniels, M. C. Strain, O. Farkas, D. K. Malick, A. D. Rabuck, K. Raghavachari, J. B. Foresman, J. V. Ortiz, Q. Cui, A. G. Baboul, S. Clifford, J. Cioslowski, B. B. Stefanov, G. Liu, A. Liashenko, P. Piskorz, I. Komaromi, R. L. Martin, D. J. Fox, T. Keith, M. A. Al-Laham, C. Y. Peng, A. Nanayakkara, M. Challacombe, P. M. W. Gill, B. Johnson, W. Chen, M. W. Wong, C. Gonzalez, J. A. Pople, Gaussian, Inc., Wallingford CT, **2004**.
[56] L. A. LaJohn, P. A. Christiansen, R. B. Ross, T. Atashroo, W. C. Ermler, *J. Chem. Phys.* **1987**, *87*, 2812–2824.
[57] K. G. Dyall, *Theor. Chem. Acc.* **1998**, *99*, 366–371.
[58] J. A. Kerr in *Handbook of Chemistry and Physics, 81st ed.* (Ed.: D. R. Lide), CRC, Boca Raton, **2000**.
[59] T. J. Volz, D. A. Rock, J. P. Jones, *J. Am. Chem. Soc.* **2002**, *124*, 9724–9725.

Received: November 28, 2006
Published online: March 19, 2007

